





Marginal Fermi liquid at magnetic quantum criticality from dimensional confinementBernhard Frank ¹, Zi Hong Liu ², Fakher F. Assaad,² Matthias Vojta,¹ and Lukas Janssen ¹¹*Institut für Theoretische Physik and Würzburg-Dresden Cluster of Excellence ct.qmat, Technische Universität Dresden, 01062 Dresden, Germany*²*Institut für Theoretische Physik und Astrophysik and Würzburg-Dresden Cluster of Excellence ct.qmat, Universität Würzburg, 97074 Würzburg, Germany* (Received 13 January 2023; revised 24 May 2023; accepted 15 August 2023; published 26 September 2023)

Metallic quantum criticality is frequently discussed as a source for non-Fermi liquid behavior, but controlled theoretical treatments are scarce. Here we identify and study a novel magnetic quantum critical point in a two-dimensional antiferromagnet coupled to a three-dimensional environment of conduction electrons. Using sign-problem-free quantum Monte Carlo simulations and an effective field-theory analysis, we demonstrate that the quantum critical point is characterized by marginal Fermi liquid behavior. In particular, we compute the electrical resistivity for transport across the magnetic layer, which effectively acts like a Kondo impurity. Due to the presence of the marginal Fermi liquid excitations, the resistivity exhibits a linear decrease with temperature at criticality, in contrast to the usual quadratic decrease. Experimental realizations in Kondo heterostructures are discussed.

DOI: [10.1103/PhysRevB.108.L100405](https://doi.org/10.1103/PhysRevB.108.L100405)

Non-Fermi liquid behavior, including that of strange metals, is often observed in correlated metals, but despite intense recent research [1–3], its origins remain poorly understood. Conceptually, one needs to distinguish cases where a description in terms of electronic quasiparticles remains valid, with potentially singular corrections to observables arising from their scattering, from those where electronic quasiparticles cease to be well-defined. The boundary between the two has been dubbed marginal Fermi liquid, characterized by a linear-in-energy scattering rate [4,5]. Deviations from Fermi-liquid behavior may occur in stable phases of matter, driven by either strong interactions, quenched disorder, or a combination of both, or it may originate from zero-temperature transitions between different quantum phases and the associated fluctuations [6–8]. The latter, referred to as metallic quantum criticality, has been studied experimentally in a variety of heavy-fermion metals [9], in ³He bilayers [10], and, most recently, in MoTe₂/WSe₂ moiré heterostructures [11]. Theoretical investigations date back to the work of Hertz [12], Millis [13], and Moriya [14], who used a perturbative framework in the spirit of Landau-Ginzburg-Wilson (LGW) to capture the physics of order-parameter fluctuations and their effects on electronic properties. Subsequent work showed that the LGW treatment is insufficient in two space dimensions, and more refined theories have been considered [2,15,16]. Their predictions have been compared to the results of extensive quantum Monte Carlo (QMC) simulations, with partial success [17]. A common problem of many simulations is that it is difficult to reach sufficiently low temperatures to access the asymptotic quantum critical regime. In this paper, we identify an example for a metallic quantum phase transition that is both analytically and computationally tractable, and realizes a novel instance of a marginal Fermi liquid. This is achieved by dimensional mismatch [18,19]: We consider a Kondo-lattice-type model [20] describing a two-dimensional

(2D) local-moment magnet embedded in a three-dimensional (3D) metal. Such a setting has been proposed in Ref. [21] and may be experimentally realized in heterostructures of layered materials, such as a single CeIn₃ layer embedded in bulk LaIn₃ [22]. Importantly, the Kondo interaction between the two subsystems suppresses magnetic order and hence enables one to tune the 2D magnet to a quantum critical point. At this critical point, the heavy quasiparticles acquire a marginal Fermi-liquid self-energy, and the electrical resistivity measured across the magnetic layer has a linear temperature dependence at low T (see Fig. 1).

Model. We model the Kondo heterostructure [Fig. 1(a)] by the Hamiltonian [21]

$$H = \sum_{k,\sigma} \epsilon_k c_{k\sigma}^\dagger c_{k\sigma} + J_H \sum_{\langle i,j \rangle} \hat{S}_i^f \cdot \hat{S}_j^f + J_K \sum_i \hat{S}_{i,R_z=0}^c \cdot \hat{S}_i^f, \quad (1)$$

with 3D conduction-electron dispersion $\epsilon_k = -2t(\cos k_x + \cos k_y + \cos k_z)$, at half filling. \hat{S}_i^f describes local spin-1/2 degrees of freedom that reside on the sites of the square lattice i in the layer at $R_z = 0$ and interact via a fixed nearest-neighbor Heisenberg coupling $J_H = t/2$. The last term parametrized by J_K describes the Kondo interaction between the local moments and the spin density of the conduction electrons $\hat{S}_{i,R_z=0}^c = 1/2 \sum_{\sigma,\sigma'} c_{i,R_z=0,\sigma}^\dagger \sigma_{\sigma\sigma'} c_{i,R_z=0,\sigma'}$ within the layer $R_z = 0$. The presence of the local moments breaks momentum conservation in the out-of-plane direction, such that k_z is not a good quantum number, whereas the in-plane momentum $\mathbf{k}_2 = (k_x, k_y)$ is conserved.

The model has been studied previously using sign-problem-free QMC simulations [21,23]. It forms an antiferromagnetic (AFM) heavy-fermion metal for small J_K and undergoes a continuous quantum phase transition to a paramagnetic heavy-fermion metal at the critical coupling

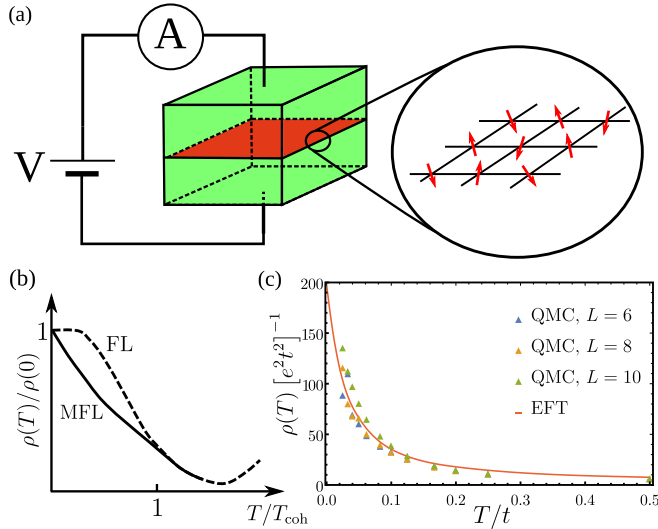


FIG. 1. (a) Schematic setup of proposed transport experiment on Kondo heterostructure. (b) Schematic temperature dependence of resistivity $\rho(T)$. The marginal Fermi liquid at the quantum critical point gives rise to a linear decrease with temperature for temperatures below the coherence scale T_{coh} , in contrast to the conventional quadratic decrease in case of a Fermi liquid. At larger temperatures beyond T_{coh} , intrinsic interaction effects in the metal lead to an increase of $\rho(T)$ (dashed line). (c) Resistivity at the quantum critical point from effective field theory and QMC simulations, both indicating the expected linear scaling and very good quantitative agreement.

$J_K^c/t = 3.019(4)$. In particular, the dimensional mismatch gives rise to a metallic ground state despite the presence of particle-hole symmetry, which entails Kondo insulators in spatially homogeneous systems. The absence of Kondo breakdown is indicated by a finite spectral weight of the composite fermion [20] $\psi_{i,\sigma}^\dagger = \sum_{\sigma'} c_{i,R_z=0,\sigma}^\dagger \sigma_{\sigma\sigma'} \cdot \hat{S}_i^f$ at small energies below the coherence scale T_{coh} throughout the phase diagram. Therefore, Ref. [21] concluded that the quantum critical point (QCP) can be described in a Landau-Ginzburg-Wilson setup, with a dynamical exponent $z = 2$. In the following, we set up an effective field theory to analyze the effect of the critical fluctuations on the fermion excitations, which are shown to exhibit marginal Fermi liquid behavior [7].

Field theory. The properties of the quantum critical regime at finite temperature can be described in terms of an imaginary-time Bose-Fermi action,

$$\begin{aligned}
 S = & \frac{1}{2} \sum_{\Omega_n, \mathbf{q}_2} \Phi_{\Omega_n, \mathbf{q}_2} \cdot D_0^{-1}(\Omega_n, \mathbf{q}_2) \Phi_{-\Omega_n, -\mathbf{q}_2} \\
 & + \sum_{\omega_n, \mathbf{k}_2, \sigma} \bar{\psi}_{\omega_n, \mathbf{k}_2, \sigma} [G_{\psi\psi}^{(0)}]^{-1} \psi_{\omega_n, \mathbf{k}_2, \sigma} \\
 & + 2g_{\text{eff}} \int_0^\beta d\tau \sum_i S_i^\psi(\tau) \cdot \Phi_i(\tau). \quad (2)
 \end{aligned}$$

The critical fluctuations of the AFM order parameter are incorporated by the real bosonic field Φ with Matsubara frequencies Ω_n . The Grassmann fields ψ and $\bar{\psi}$ represent the composite fermions, with Matsubara frequencies ω_n , which dominate the fermion density of states at criticality [21].

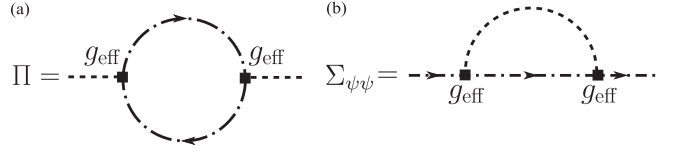


FIG. 2. Self-energy for (a) order-parameter and (b) fermion fields. Dashed internal lines correspond to D propagators and dotted-dashed ones to $G_{\psi\psi}$ propagators. Squares denote the effective interaction strength g_{eff} .

The effective coupling g_{eff} considers only the most relevant interaction between the AFM fluctuations and the spin density of the composite fermions $S_i^\psi = 1/2 \sum_{\sigma, \sigma'} \bar{\psi}_{i,\sigma} \sigma_{\sigma\sigma'} \psi_{i,\sigma'}$. Similar models have been discussed in various contexts, describing, e.g., conduction electrons coupled to ferromagnetic [24,25], Ising-nematic [26–28], or antiferromagnetic [16,29,30] order parameters, as well as to a U(1) gauge field [31–33]. In two dimensions, these setups can potentially host non-Fermi liquid states, characterized by the lack of well-defined quasiparticles [2,7]. Importantly, the critical fluctuations may alter the behavior of the fermion excitations beyond the well-established Hertz-Millis theory [12–14], which considers only the dressing of the order-parameter fluctuations by correlations of essentially noninteracting electrons. In the above equation, the bare fermionic propagator includes the mean-field hybridization effects,

$$\begin{aligned}
 G_{\psi\psi}^{(0)}(\omega_n, \mathbf{k}_2) &= \frac{4}{J_K^2} \tilde{T}_{\text{MF}}(\omega_n, \mathbf{k}_2) \\
 &= \frac{4J_K^{-2}}{v_{\text{MF}}^{-2} i\omega_n - \tilde{\epsilon}_{\mathbf{k}_2} - g_0(\omega_n, \mathbf{k}_2)}, \quad (3)
 \end{aligned}$$

in terms of the mean-field transition matrix \tilde{T}_{MF} , encoding the out-of-plane scattering of conduction electrons off the spin layer. Here, we introduce $g_0(\omega_n, \mathbf{k}_2) = 1/(\sqrt{i\omega_n - \epsilon_{\mathbf{k}_2} + 2t} \sqrt{i\omega_n - \epsilon_{\mathbf{k}_2} - 2t})$ with in-plane dispersion $\epsilon_{\mathbf{k}_2} = -2t(\cos k_x + \cos k_y)$, while $v_{\text{MF}}^{-2} i\omega_n - \tilde{\epsilon}_{\mathbf{k}_2}$ incorporates the Kondo resonances from screening the local moments with weights v_{MF}^2 and dispersion $\tilde{\epsilon}_{\mathbf{k}_2} = (t'/t)\epsilon_{\mathbf{k}_2}$. The derivation of Eq. (3) and a comparison with QMC data are given in the Supplemental Material (SM) [34]. Furthermore, we model the bare antiferromagnetic susceptibility with the standard asymptotic form $D^{(0)}(\Omega_n, \mathbf{q}_2) = (\Omega_n^2 + c_B^2(\mathbf{q}_2 - \mathbf{Q})^2 + M_0^2)^{-1}$, with instability wave vector $\mathbf{Q} = (\pi, \pi)$ and boson velocity c_B . M_0^2 describes the bare spectral gap. Interactions dress the propagators via self-energies Π and $\Sigma_{\psi\psi}$ as $D(\Omega_n, \mathbf{q}_2) = [D^{(0)}(\Omega_n, \mathbf{q}_2)^{-1} + \Pi(\Omega_n, \mathbf{q}_2)]^{-1}$ and $G_{\psi\psi} = 4/J_K^2 [\tilde{T}_{\text{MF}}^{-1} - (4/J_K)^2 \Sigma_{\psi\psi}]^{-1}$. At the QCP, the gap vanishes, $M^2 \equiv M_0^2 + \Pi(\Omega = 0, \mathbf{Q}) = 0$, while a finite value $M^2 > 0$ ($M^2 < 0$) drives the system into the paramagnetic (antiferromagnetic) heavy-fermion metal. In the following, we perform a one-loop analysis that captures the most important interaction effects; see Figs. 2(a) and 2(b) for corresponding diagrams.

Results at $T = 0$. We start with the behavior at the QCP. Note that $G_{\psi\psi}^{(0)}$ does not exhibit the typical free-particle poles in the vicinity of the Fermi surface. Instead, only a discontinuity appears at in-plane momenta \mathbf{k}_2 within the projected

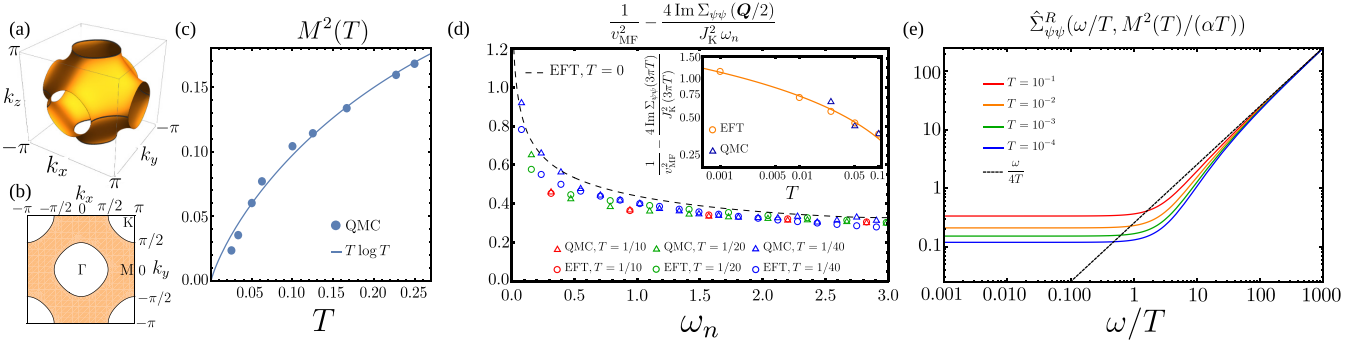


FIG. 3. (a) 3D Fermi surface. (b) Projected 2D Fermi surface. (c) Thermal gap as a function of temperature from Hertz-Millis asymptotics $M^2(T) \sim T \log T$ (solid line) and QMC at linear system size $L = 12$ (dots). (d) Imaginary part of fermionic self-energy as a function of Matsubara frequency from effective field theory (triangles) and $L = 12$ QMC (dots) for different temperatures. The black dashed line corresponds to the result at $T = 0$. The inset shows the variation at the Matsubara frequency $\omega_n = 3\pi T$ as a function of temperature, which follows a logarithmic asymptotics (solid line). (e) Imaginary part of retarded fermionic self-energy as a function of real frequency ω from effective field theory.

2D Fermi surface, shown in Fig. 3(b). This more regular infrared behavior has important consequences for the critical properties. The evaluation of Fig. 2(a) leads to the dressed boson propagator at criticality as [34]

$$D(\Omega, \mathbf{q}_2) = \frac{1}{c_B^2(\mathbf{q}_2 - \mathbf{Q})^2 + \alpha|\Omega|}, \quad (4)$$

with the nonanalyticity, parametrized by the nonuniversal prefactor α , representing Landau damping, in a form typically encountered in AFM metallic QCPs [12]. It implies a dynamical exponent $z = 2$, in agreement with the QMC results [21]. For the fermion self-energy, we find from Fig. 2(b), using the dressed boson propagator [34],

$$\Sigma_{\psi\psi}(\omega, \mathbf{k}_2) = -i\gamma(\epsilon_{\mathbf{k}_2})\omega \log\left(\frac{e^2\Lambda^2}{\alpha|\omega|}\right), \quad (5)$$

which holds for \mathbf{k}_2 within the projected 2D Fermi surface. Here, $\gamma(\epsilon_{\mathbf{k}_2})$ denotes a nonuniversal momentum-dependent prefactor and Λ is the momentum cutoff. Analytic continuation $\Sigma_{\psi\psi}(i\omega \rightarrow \omega + i0^+)$ to real frequencies yields the retarded self-energy $\Sigma_{\psi\psi}^R$ whose imaginary part encodes the decay rate of the single-particle excitations. For the Kondo heterostructure, we find $-\text{Im}\Sigma_{\psi\psi}^R(\omega, \mathbf{k}_2) \sim |\omega|$, which implies marginal-Fermi-liquid scaling. We note that the notion of marginal Fermi liquidity was historically based on the concept of local charge and spin responses [4]. However, as we demonstrate in the SM [34], in our setup, featuring dimensional mismatch, the charge and spin responses are local not only in the marginal Fermi liquid state, but also in the standard Fermi liquid, and as such are not characteristic of non-Fermi liquid behavior. In our work, we therefore use the more recent understanding of the concept of a marginal Fermi liquid that is based on the decay of the single-particle excitations and their scaling with energy [35–41]. The unusual scaling originates from the discontinuity of $G_{\psi\psi}^{(0)}$ and differs from the decay rate $\sim |\omega|^{1/2}$ obtained in the case of a critical AFM order parameter coupled to a 2D Fermi surface [29].

In addition to these perturbative results, we can make precise statements about the universality class of the bosonic sector of the Kondo heterostructure, which typically is a hard

problem in metallic quantum criticality. In the present case with dimensional mismatch, higher-order vertex functions beyond the quartic interaction turn out to be renormalization-group irrelevant, such that the bosonic sector is described by Hertz-Millis scaling with dynamical critical exponent $z = 2$ in $d = 2$ spatial dimensions (see SM for details [34]). The resulting scaling relations [13] affect the behavior of the marginal-Fermi-liquid self-energy $\Sigma_{\psi\psi}$ at finite temperatures, as discussed next.

Finite temperature and comparison with QMC. We follow the procedure developed in Ref. [42] and compute $\Sigma_{\psi\psi}(\omega_n, \mathbf{k}_2)$ self-consistently at the one-loop level, to capture thermal effects properly, while we use numerical input from the QMC simulations to set the values of the nonuniversal parameters characterizing the dressed propagators. For instance, in the case of the boson propagator, in the vicinity of the instability wave vector $\mathbf{Q} = (\pi, \pi)$, we expect an asymptotic behavior,

$$D(\Omega_n, \mathbf{q}_2) = \frac{1}{d_0^{-1}\Omega_n^2 + c_B^2(\mathbf{q}_2 - \mathbf{Q})^2 + M^2(T) + \alpha|\Omega_n|}, \quad (6)$$

where we have introduced, in addition to the Landau damping, an analytic frequency dependence with nonuniversal prefactor d_0^{-1} and an effective finite-temperature gap $M^2(T)$, realizing the thermal cutoff, with $M^2(0) = 0$. In general, $M^2(T)$ may realize a rather rich behavior as a function of temperature [43]. Here, however, Hertz-Millis scaling dictates the form $M^2(T) \sim T \log T$, which agrees well with the QMC results [see Fig. 3(c)]. This allows us to fix all nonuniversal parameters in the bosonic sector uniquely. Similarly, the renormalized hopping amplitude t'/t of the Kondo resonances can be extracted directly from the QMC results for the propagator of the conduction electrons. The weight of the resonances v_{MF}^2 , as well as the fermion-boson coupling g_{eff} , can be obtained by matching the self-consistent result for $\Sigma_{\psi\psi}(\omega_n, \mathbf{Q})$ at a fixed temperature, which we choose as $T/t = 1/10$ (see SM [34] for details). To compare with the effective field theory, we use the identity $\text{Im}[\tilde{T}(\omega_n, \mathbf{k}_2) - g_0(\omega_n, \mathbf{k}_2)] = v_{\text{MF}}^{-2}\omega_n - 4J_{\text{K}}^{-2}\text{Im}\Sigma_{\psi\psi}(\omega_n, \mathbf{k}_2)$. The left-hand side can be extracted directly from the QMC data while the right-hand side is

obtained from the effective field theory. To enhance the resolution we divide by ω_n . The resulting agreement between the effective field theory and the QMC data for the fermionic self-energy as a function of the Matsubara frequency ω_n for different temperatures and linear system size $L = 12$ is remarkable [see Fig. 3(d)]. This includes the correction to the linear behavior in general, as well as the pronounced increase at the smallest ω_n . Importantly, the effective field theory allows us to extrapolate to lower temperatures down to $T = 0$. As revealed in Fig. 3(d), this limit is approached only logarithmically with decreasing temperature.

Transport. Finally, we address the question how the marginal Fermi liquid can be observed experimentally. Since the Kondo interactions are restricted to the spin layer, they do not affect the bulk thermodynamic properties of the conduction electrons. Transport across the spin plane, however, is sensitive to the presence of the local moments. In the following, we consider a simple setup in which the region above the spin plane, $R_z > 0$, is subject to a static homogeneous electric potential, $eV > 0$. By symmetry, only a uniaxial, stationary current density along the positive out-of-plane direction $\langle J^z \rangle$ will be generated. Within linear response, the conductivity σ is given by Ohm's law $\langle J^z \rangle = \sigma V / (2a)$, where $a = 1$ is the lattice constant [44]. The calculation of σ is tremendously simplified by the conservation of in-plane momenta, which allows us to theoretically decompose the Kondo heterostructure into L^2 -independent one-dimensional scattering problems, labeled by \mathbf{k}_2 . Each of these realizes an interacting quantum dot in the layer $R_z = 0$, connected to two identical leads formed by the noninteracting regions $R_z < 0$ and $R_z > 0$, respectively. For a fixed \mathbf{k}_2 , the conductivity can, therefore, be obtained via the Meir-Wingreen formalism [45]. As is derived in detail in Ref. [34], the total conductivity is obtained by summing the Meir-Wingreen result over \mathbf{k}_2 :

$$\sigma = -4\pi e^2 t^2 \int \frac{d^2 k_2}{(2\pi)^2} d\omega a_0(\omega, \mathbf{k}_2) n'_F(\omega) \Big|_{\mu=0} a(\omega, \mathbf{k}_2). \quad (7)$$

In the above, $n'_F(\omega) = dn_F(\omega)/d\omega$ denotes the derivative of the Fermi distribution and $a_0(\omega, \mathbf{k}_2) = -\pi^{-1} \text{Im} g_0(i\omega_n \rightarrow \omega + i0^+, \mathbf{k}_2)$ is the free one-dimensional density of states of the leads. The only genuine interaction contribution is given by the dressed local spectral function of the conduction electrons $a(\omega, \mathbf{k}_2) = -\pi^{-1} \text{Im} g(i\omega_n \rightarrow \omega + i0^+, \mathbf{k}_2)$ that derives from the dressed local Green's function [34]. At $T = 0$, the conductivity attains a nonuniversal value, $\sigma(T = 0)$, which originates from scattering off conduction electrons from the Kondo-screened local moments. However, the deviation $\delta\sigma(T) = \sigma(T) - \sigma(0)$ shows the same temperature dependence as the imaginary part of the analytically continued retarded self-energy $\text{Im} \Sigma_{\psi\psi}^R$, implying that the conductivity is sensitive to the nature of the composite fermion excitations and their marginal-Fermi-liquid behavior. The diagrammatic evaluation [34] reveals that the frequency and temperature dependence of the retarded self-energy can be expressed as $\text{Im} \Sigma_{\psi\psi}^R(\omega, \mathbf{k}_2) \sim T \hat{\Sigma}_{\psi\psi}^R(\omega/T, M^2(T)/\alpha T)$, where $\hat{\Sigma}_{\psi\psi}^R$ is a momentum-independent, universal scaling function [see Fig. 3(e)]. In the quantum critical regime, we obtain two different limiting behaviors: (i) For large frequencies $|\omega|/T \gg 1$,

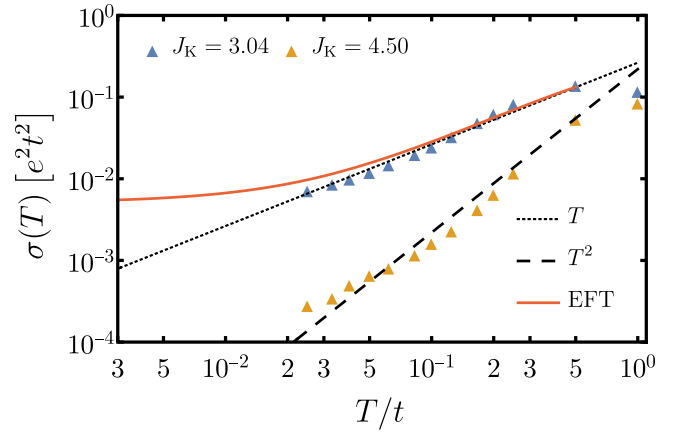


FIG. 4. Conductivity as a function of temperature from effective field theory at criticality (red solid line) and QMC simulations for $J_K = 3.04t \approx J_K^c$ (blue triangles) and $J_K = 4.50t > J_K^c$ (yellow triangles) for linear system size $L = 10$. The black dotted (dashed) line indicates the linear (quadratic) marginal-Fermi-liquid (Fermi-liquid) scaling.

we have $\hat{\Sigma}_{\psi\psi}^R \sim |\omega|/T$, such that $\text{Im} \Sigma_{\psi\psi}^R \sim |\omega|$ recovers the marginal-Fermi-liquid behavior from the QCP, as expected; and (ii) for small frequencies $|\omega|/T \ll 1$, we obtain a constant $\hat{\Sigma}_{\psi\psi}^R(0, M^2(T)/\alpha T)$, which scales like $T^2/M^2(T) \sim T/\log T$ in the limit of small temperatures. Since the overall scale of the self-energy is set by the temperature, we obtain $\delta\sigma(T) \sim T$ up to logarithmic corrections (see Fig. 4). Converted to the resistivity $\rho(T) = 1/\sigma(T)$, these results imply a linear decrease with temperature for temperatures below the coherence scale T_{coh} , as schematically indicated in Fig. 1(b). In the paramagnetic heavy-fermion metal at sufficiently large J_K , we find instead the Fermi-liquid self-energy $\text{Im} \Sigma^R(\omega, \mathbf{k}_2) \sim \max(\omega^2, T^2)$, resulting in $\delta\sigma(T) \sim T^2$, implying the conventional form of $\rho(T)$ at low temperatures [46], as also indicated in Fig. 1(b).

The conductivity may be also accessed from the QMC simulations without numerical analytic continuation, provided that one approximates $n'_F(\omega) \approx -\delta(\omega)$. Such replacement neither affects the temperature scaling nor introduces a large numerical error (see Ref. [34]). The value of $a(\omega = 0, \mathbf{k}_2)$ at a single real frequency can then be obtained from the QMC data at imaginary times in a controlled way for $T \rightarrow 0$. Figure 4 shows that the QMC simulations indeed display the expected linear (quadratic) scaling for $J_K \approx J_K^c$ ($J_K > J_K^c$). Moreover, at criticality, we even find very good quantitative agreement between the QMC data and the effective field theory. This is also reflected in the resistance as a function of temperature at the quantum critical point, as presented in Fig. 1(c).

Summary. We have identified a quantum critical point in a model for a Kondo heterostructure, which realizes a novel instance of a marginal Fermi liquid, characterized by a linear temperature dependence of the electrical resistivity measured across the magnetic layer. Our results call for careful low-temperature transport experiments on appropriate heterostructures made of single magnetic layers embedded in bulk metals, which can be tuned close to a quantum critical point. In this respect, we note that various heavy-fermion compounds, such as bulk CeIn_3 , feature a pressure-driven

quantum phase transition [47], suggesting that pressurized $\text{CeIn}_3/\text{LaIn}_3$ [22] or related heterostructures could realize some of the physics discussed in this work. On a more general note, our work provides a path to engineer, and characterize in transport experiments, exotic quantum phases of matter using the concept of dimensional mismatch.

Acknowledgments. F.A. and M.V. acknowledge enlightening conversations with T. Grover and B. Danu on related subjects. The authors gratefully acknowledge the Gauss Centre for Supercomputing e.V. [56] for funding this project by providing computing time on the GCS Supercomputer SUPERMUC-NG at the Leibniz Supercomputing Centre [57], (Grant No. pn73xu) as well as the scientific support and HPC resources provided by the Erlangen National

High Performance Computing Center (NHR@FAU) of the Friedrich-Alexander-Universität Erlangen-Nürnberg (FAU) under the NHR Grant No. b133ae. NHR funding is provided by federal and Bavarian state authorities. NHR@FAU hardware is partially funded by the Deutsche Forschungsgemeinschaft (DFG) (DFG Grant No. 440719683). This research has been supported by the DFG through the Würzburg-Dresden Cluster of Excellence on Complexity and Topology in Quantum Matter—*ct.qmat* (EXC 2147, Grant No. 390858490), SFB 1170 on Topological and Correlated Electronics at Surfaces and Interfaces (Grant No. 258499086), SFB 1143 on Correlated Magnetism (Grant No. 247310070), and the Emmy Noether Program (JA2306/4-1, Grant No. 411750675).

-
- [1] G. R. Stewart, *Rev. Mod. Phys.* **73**, 797 (2001).
- [2] S.-S. Lee, *Annu. Rev. Condens. Matter Phys.* **9**, 227 (2018).
- [3] P. W. Phillips, N. E. Hussey, and P. Abbamonte, *Science* **377**, 169 (2022).
- [4] C. M. Varma, P. B. Littlewood, S. Schmitt-Rink, E. Abrahams, and A. E. Ruckenstein, *Phys. Rev. Lett.* **63**, 1996 (1989).
- [5] C. M. Varma, Z. Nussinov, and W. van Saarloos, *Phys. Rep.* **361**, 267 (2002).
- [6] S. Sachdev, *Quantum Phase Transitions*, 2nd ed. (Cambridge University, Cambridge, England, 2011).
- [7] H. v. Löhneysen, A. Rosch, M. Vojta, and P. Wölfle, *Rev. Mod. Phys.* **79**, 1015 (2007).
- [8] P. Gegenwart, Q. Si, and F. Steglich, *Nat. Phys.* **4**, 186 (2008).
- [9] S. Wirth and F. Steglich, *Nat. Rev. Mater.* **1**, 16051 (2016).
- [10] M. Neumann, J. Nyéki, B. Cowan, and J. Saunders, *Science* **317**, 1356 (2007).
- [11] W. Zhao, B. Shen, Z. Tao, Z. Han, K. Kang, K. Watanabe, T. Taniguchi, K. F. Mak, and J. Shan, *Nature (London)* **616**, 61 (2023).
- [12] J. A. Hertz, *Phys. Rev. B* **14**, 1165 (1976).
- [13] A. J. Millis, *Phys. Rev. B* **48**, 7183 (1993).
- [14] T. Moriya, *Spin Fluctuations in Itinerant Electron Magnetism* (Springer, Berlin, 2012).
- [15] A. Abanov and A. Chubukov, *Phys. Rev. Lett.* **93**, 255702 (2004).
- [16] A. Schliefl, P. Lunts, and S.-S. Lee, *Phys. Rev. X* **7**, 021010 (2017).
- [17] E. Berg, S. Lederer, Y. Schattner, and S. Trebst, *Annu. Rev. Condens. Matter Phys.* **10**, 63 (2019).
- [18] B. Danu, M. Vojta, F. F. Assaad, and T. Grover, *Phys. Rev. Lett.* **125**, 206602 (2020).
- [19] B. Danu, M. Vojta, T. Grover, and F. F. Assaad, *Phys. Rev. B* **106**, L161103 (2022).
- [20] B. Danu, Z. Liu, F. F. Assaad, and M. Raczkowski, *Phys. Rev. B* **104**, 155128 (2021).
- [21] Z. H. Liu, B. Frank, L. Janssen, M. Vojta, and F. F. Assaad, *Phys. Rev. B* **107**, 165104 (2023).
- [22] H. Shishido, T. Shibauchi, K. Yasu, T. Kato, H. Kontani, T. Terashima, and Y. Matsuda, *Science* **327**, 980 (2010).
- [23] F. F. Assaad, M. Bercx, F. Goth, A. Götz, J. S. Hofmann, E. Huffman, Z. Liu, F. P. Toldin, J. S. E. Portela, and J. Schwab, *SciPost Phys. Codebases* **1** (2022).
- [24] A. V. Chubukov, C. Pépin, and J. Rech, *Phys. Rev. Lett.* **92**, 147003 (2004).
- [25] A. V. Chubukov and D. L. Maslov, *Phys. Rev. Lett.* **103**, 216401 (2009).
- [26] W. Metzner, D. Rohe, and S. Andergassen, *Phys. Rev. Lett.* **91**, 066402 (2003).
- [27] L. Dell'Anna and W. Metzner, *Phys. Rev. B* **73**, 045127 (2006).
- [28] M. A. Metlitski and S. Sachdev, *Phys. Rev. B* **82**, 075127 (2010).
- [29] A. Abanov, A. V. Chubukov, and J. Schmalian, *Adv. Phys.* **52**, 119 (2003).
- [30] M. A. Metlitski and S. Sachdev, *Phys. Rev. B* **82**, 075128 (2010).
- [31] P. A. Lee, *Phys. Rev. Lett.* **63**, 680 (1989).
- [32] B. L. Altshuler, L. B. Ioffe, and A. J. Millis, *Phys. Rev. B* **50**, 14048 (1994).
- [33] S.-S. Lee, *Phys. Rev. B* **80**, 165102 (2009).
- [34] See Supplemental Material at <http://link.aps.org/supplemental/10.1103/PhysRevB.108.L100405> for details on the structure of the fermion propagators, the mean-field form of the T matrix, details on the evaluation of the one-loop self-energies, an analysis of the momentum dependencies of the spin and charge correlators, the characterization of the universality class of the bosonic sector, details on the comparison between analytical and QMC results, and the derivation of the conductivity via the Meir-Wingreen formalism, which includes Refs. [48–55].
- [35] J. González, F. Guinea, and M. A. H. Vozmediano, *Phys. Rev. B* **59**, R2474 (1999).
- [36] T. Senthil, *Phys. Rev. B* **78**, 045109 (2008).
- [37] S. Jia, P. Jiramongkolchai, M. R. Suchomel, B. H. Toby, J. G. Checkelsky, N. P. Ong, and R. J. Cava, *Nat. Phys.* **7**, 207 (2011).
- [38] A. A. Patel, J. McGreevy, D. P. Arovas, and S. Sachdev, *Phys. Rev. X* **8**, 021049 (2018).
- [39] E. E. Aldape, T. Cookmeyer, A. A. Patel, and E. Altman, *Phys. Rev. B* **105**, 235111 (2022).
- [40] H. Guo, A. A. Patel, I. Esterlis, and S. Sachdev, *Phys. Rev. B* **106**, 115151 (2022).
- [41] A. A. Patel, H. Guo, I. Esterlis, and S. Sachdev, *Science* **381**, 790 (2023).
- [42] A. Klein, A. V. Chubukov, Y. Schattner, and E. Berg, *Phys. Rev. X* **10**, 031053 (2020).

- [43] B. Frank and F. Piazza, [arXiv:2011.07076](https://arxiv.org/abs/2011.07076).
- [44] This setup neglects intrinsic defects within the metals, which break translation invariance on the microscopic level and affect the homogeneity of $\langle J^z \rangle$. For good metals these effects are expected to be subleading for large enough sample sizes. Furthermore, intrinsic interactions of the electrons within the metallic regions $R_z \neq 0$ are not considered. These lead to an increase of $\rho(T)$ with increasing temperature as depicted schematically in Fig. 1(b).
- [45] Y. Meir and N. S. Wingreen, *Phys. Rev. Lett.* **68**, 2512 (1992).
- [46] P. Nozières, *J. Low Temp. Phys.* **17**, 31 (1974).
- [47] N. D. Mathur, F. M. Grosche, S. R. Julian, I. R. Walker, D. M. Freye, R. K. W. Haselwimmer, and G. G. Lonzarich, *Nature (London)* **394**, 39 (1998).
- [48] B. Mihaila, [arXiv:1111.5337](https://arxiv.org/abs/1111.5337).
- [49] L. Borda, L. Fritz, N. Andrei, and G. Zaránd, *Phys. Rev. B* **75**, 235112 (2007).
- [50] A. L. Fetter and J. D. Walecka, *Quantum Theory of Many-Particle Systems* (McGraw-Hill, Boston, 1971).
- [51] M. E. Peskin and D. V. Schroeder, *An Introduction to Quantum Field Theory* (Addison-Wesley, Reading, MA, 1995).
- [52] A. Altland and B. D. Simons, *Condensed Matter Field Theory*, 2nd ed. (Cambridge University Press, Cambridge, England, 2010).
- [53] J. R. Iglesias, C. Lacroix, and B. Coqblin, *Phys. Rev. B* **56**, 11820 (1997).
- [54] C. Caroli, R. Combescot, P. Nozieres, and D. Saint-James, *J. Phys. C* **4**, 916 (1971).
- [55] K. Beach, [arXiv:cond-mat/0403055](https://arxiv.org/abs/cond-mat/0403055).
- [56] Gauss Centre for Supercomputing e.V., www.gauss-centre.eu.
- [57] Leibniz Supercomputing Centre, www.lrz.de.